ELSEVIER

Chemical Physics 266 (2001) 237–250

Chemical Physics

www.elsevier.nl/locate/chemphys

Two-dimensional spectroscopy and harmonically coupled anharmonic oscillators

Ko Okumura [a,*], David M. Jonas [b], Yoshitaka Tanimura [c]

[a] *Department of Physics, Faculty of Science, Ochanomizu University, Bunkyo, Tokyo 112-8610, Japan*
[b] *Department of Chemistry and Biochemistry, University of Colorado, Boulder, CO 80309-0215, USA*
[c] *Theoretical Studies, Institute for Molecular Science, Okazaki, Aichi 444-8585, Japan*

Received 20 October 2000

Abstract

Experimentally it is established that the fourth-order anharmonicity plays significant roles in many molecules. In high resolution spectroscopy, it is known that a picture of local (anharmonic) modes with harmonic couplings between modes gives rise to a quartic Darling–Dennison coupling between normal modes. It has been shown that this order of anharmonicity can be selectively studied via seventh-order off-resonant spectroscopy, which probes the three-time response function (J. Chem. Phys. 106 (1997) 1687). In this paper, we further explore the effect of the fourth-order anharmonicity in the seventh-order signal, or in the three-time response function (which can be complementary investigated via third-order infrared spectroscopy), when the anharmonicity causes mode mixing; we obtain a fairly compact analytical result and numerically present the signal from CH stretch vibrations in methylene chloride as two-dimensional (2D) contour maps. It is found that purely kinetic coupling between anharmonic local oscillators can give rise to cross-peaks in the 2D spectra.

1. Introduction

The two-dimensional (2D) laser spectroscopy has recently been explored by many groups. This laser analogue of the NMR spectroscopy has long been overdue; the experimental and theoretical sophistication has reached the level required to the realization.

One of the pioneering works for the optical analogue was the work [1] on the fifth-order off-resonant processes, where a possible discrimination of inhomogeneity from homogeneity in liquid spectroscopy was demonstrated. This work motivated a few groups to overcome experimental difficulties toward the detection of the fifth-order signal [2–4]. Possible important origins of the signals in the fifth-order spectroscopy, i.e. anharmonicity (in potential) and nonlinearity (in polarizability), were pointed out in Refs. [5,6]. Anharmonicity and nonlinearity then became key ideas in experimental interpretations of the fifth-order Raman spectroscopy. This picture was tested with the aid of ab initio calculation [7] and anharmonicity was further examined in Refs. [8,9]. Another issue brought up next was the mode coupling [10,11] in the frequency domain. After some discussions of the cascading effect [12–14], new experimental results [15–18] on the low frequency modes of liquid CS_2 are ready for comparison to molecular level calculations [19–22].

* Corresponding author.
E-mail address: okumura@phys.ocha.ac.jp (K. Okumura).

0301-0104/01/$ - see front matter
PII: S0301-0104(01)00252-X

In parallel with this high level of activity in 2D Raman spectroscopy, researchers have explored the 2D spectroscopy in a broader context (second harmonic generation [23], resonant spectroscopy [24–27], CW spectroscopy [28–31], THz spectroscopy [32], combination of infrared and optical sources [33] etc.). The possibility of structural analysis by the optical 2D spectroscopy has been investigated theoretically [34] and has also been explored experimentally [35] by direct analogy to 2D NMR correlation spectroscopy (COSY) [36]. The theoretical demonstration has been examined by ab initio calculation [37], where effects of nonlinear system–bath coupling upon the fifth- and seventh-order Raman experiments have been investigated [38,39]. Echo phenomena in 2D Raman spectra have been revisited [40,41], and are related to investigations of the 2D line shape in resonant photon echoes [27,42,43].

In this article, we explore a new direction toward even higher order spectroscopy. It has been shown that the fifth-, seventh-, ninth-order off-resonant Raman spectroscopy has an enhanced sensitivity to third-, fourth-, fifth-order anharmonicity, respectively [6]. In this paper, we further examine the seventh-order spectroscopy and demonstrate its connection to the Darling–Dennison (D–D) anharmonic coupling, which typically results from a harmonic coupling of anharmonic oscillators.

Note here that the three-time response function detected via seventh-order Raman spectroscopy and thus studied in the present paper can be complementary observed through third-order infrared spectroscopy, as suggested in Ref. [33]. In addition, if we use optical laser in combination with infrared laser, the three-time response function can be investigated via either third-, fourth-, fifth-, sixth-, or seventh-order spectroscopy. In this sense, we should keep in mind that the present theory is not limited to the seventh-order spectroscopy.

Thus, seventh-order 2D Raman is complementary to third-order 2D infrared, and both should provide direct information about quartic anharmonic coupling between harmonic normal modes. By analogy to 2D NMR [36], the dipole–dipole coupling interaction between identical bonds has been proposed as a structural diagnostic [34,35,37]. It is therefore important to understand mechanical coupling (which includes potential coupling and kinetic coupling) between identical bonds quantitatively. Normal modes automatically incorporate any quadratic coupling between bonds exactly, so this 1:1 coupling is not reflected in 2D cross-peaks. (Here and hereafter, "*i:j* coupling" refers to an interaction where one mode loses i quanta whereas another mode gains j quanta.) 2:2 effective quartic couplings are thus one of the lowest order resonant couplings between identical bonds with the potential to appear in the 2D cross-peak spectrum. Since the work of Darling and Dennison on the overtone spectra of H_2O [44], the importance of 2:2 resonant coupling has been recognized in high resolution spectroscopy [45–49]. The zero-order picture which emerged from these studies assumes each identical bond has the same anharmonic "local mode" potential and that the dominant coupling between bonds arises from the kinetic energy [45,50]. Here, the kinetic energy coupling between bonds refers to the coupling resulting from the requirement that the center of mass remain fixed during vibration [51] and is the only coupling between bonds in a valence force field [47,52]. [1] In this way, the anharmonic nature of the individual bonds gives rise to a systematic pattern of anharmonic couplings between normal modes which depends on the atomic masses and molecular geometry [45]. It is therefore conceivable that such couplings may be structurally informative in condensed phase 2D spectroscopy.

Careful investigations of this local mode model by high resolution spectroscopy have revealed that the third-order effect of cubic anharmonicity and the second-order effect of quartic anharmonicity usually make comparable contributions to the effective quartic coupling [45,53]. Early work by Pliva [54] and the considerable success of the vibron model developed by Iachello, Levine and coworkers [55–57] indicates that bonds in many

[1] This potential coupling also generates higher order anharmonic interactions because the harmonic Cartesian potential coupling becomes anharmonic in curvilinear bond length/angle coordinates.

molecules can be well described by simple, universal potentials. (Morse oscillators for stretching vibrations, symmetrical anharmonic bending potentials.) Departures from this basic model, such as potential coupling between bonds, are considered to be higher order effects. For simplicity, the model considered here includes only the lowest order effect of bond anharmonicity on absolute value seventh-order Raman spectra. (The anharmonic potential investigated in this paper is quite general as introduced in Eq. (2) below; it includes, say, the ninth-order anharmonicity coefficient $g^{(9)}_{ij\ldots k}$. However, up to the leading order (in $g^{(m)}_{ij\ldots k}$'s), the three-time response function is insensitive to such anharmonic coefficients, $g^{(m)}_{ij\ldots k}$'s, except for $g^{(4)}_{ijkl}$). This is sufficient to demonstrate that this seventh-order 2D spectra reflect especially the quartic anharmonicity and that the relative intensities of the cross-peaks are sensitive to the systematic coupling pattern generated by kinetic coupling between identical anharmonic local oscillators.

Our argument presented below is based on the Brownian oscillator model [58]. As pointed out in Refs. [13,59,60], for the intermolecular low-frequency modes of liquid, this model might be regarded as a pragmatic one. For the intramolecular modes of liquids, however, this model is well defined and can give molecular-level understanding.

2. The three-time response function for anharmonic systems

It was suggested in Ref. [1] that the fifth-order signal is proportional to $a_1^2 a_2$ where a_i is the ith coefficient of the expansion of the molecular polarizability $\alpha(Q)$ in terms of some nuclear coordinate Q, i.e., $\alpha = a_0 + a_1 Q + a_2 Q^2 + \cdots$. It implied that detection of the signal might be difficult if the nonlinearity a_2 in polarizability was small and there is an indication from an instantaneous normal mode (INM) calculation of the polarizability-weighted density of states that a_2 is small [59,60]. However, it was shown in Refs. [5,6] that even though the nonlinearity is small, the signal might be detected with less difficulty if the third-order anharmonicity λ_3 in the potential is not small (because of the contribution proportional to $a_1^3\lambda_3$); the total fifth-order signal results from interference between the nonlinearity and the anharmonicity. Here, λ_i is the ith coefficient of the expansion of the potential energy of the vibrational mode, $V(Q)$, i.e., $V = \lambda_2 Q^2 + \lambda_3 Q^3 + \lambda_4 Q^4 + \cdots$.

In the present analysis, we calculate seventh-order signal proportional to $a_1^4\lambda_4$. Thus, even if the polarizability nonlinearity is small, one might be able to measure the signal if the quartic anharmonicity λ_4 is not small. Note here that, as written in Section 1, it is experimentally confirmed that the effective fourth-order anharmonic potential coupling has been regarded as important in some cases.

The pulse configuration of the seventh-order off-resonant signal is given in Fig. 1. The optical observable for femtosecond pulse sequences is proportional to the three-time response function [58],

$$R(T_1,T_2,T_3) = \left(\frac{\mathrm{i}}{\hbar}\right)^3 \langle[[[\alpha(T_1+T_2+T_3),\alpha(T_1+T_2)],\alpha(T_1)],\alpha(0)]\rangle.$$

The complete seventh-order response has seven time dimensions, but four off-resonant electronic time dimensions have been suppressed in the response function because they are limited to times of the order $1/(\omega_{\mathrm{eg}} - \omega_{\mathrm{L}})$ where ω_{eg} and ω_{L} are the electronic absorption and laser frequencies, respectively.

We assume that the system can be characterized by several modes represented by the coordinates Q_i, frequencies Ω_i, damping constants (=FWHM) Γ_i $(i = 1,2,\ldots)$. The potential of the system is assumed to be

$$V(Q) = V_{\mathrm{H}}(Q) + V_{\mathrm{AH}}(Q),$$

where the harmonic and anharmonic contributions are given by

$$V_{\mathrm{H}}(Q) = \frac{1}{2}\sum_i \Omega_i^2 Q_i^2, \tag{1}$$

$$V_{\mathrm{AH}}(Q) = \sum_{i,j,k} \frac{g^{(3)}_{ijk}}{3!} Q_i Q_j Q_k + \sum_{i,j,k,l} \frac{g^{(4)}_{ijkl}}{4!} Q_i Q_j Q_k Q_l + \cdots. \tag{2}$$

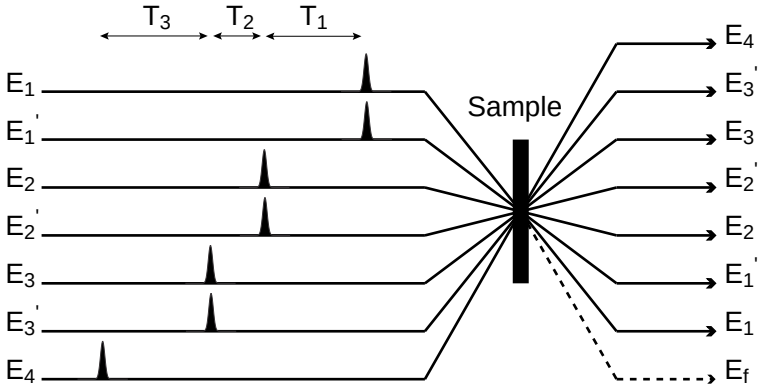

Fig. 1. Pulse configuration for the seventh-order spectroscopy. We set $T_2 = 0$ in this paper; the time-domain signal $R(T_1, T_2 = 0; T_3)$ is Fourier transformed with respect to T_1 and T_3 to the frequency-domain quantity $\bar{I}(\omega_1, \omega_3)$, where the signal is given by its absolute value.

In the system with the linear polarizability,

$$\alpha = \alpha^{(0)} + \sum_i \alpha_i^{(1)} Q_i,$$

we have

$$R(T_1, T_2, T_3) = \left(\frac{i}{\hbar}\right)^3 \sum_{i,j,k,l} \alpha_i^{(1)} \alpha_j^{(1)} \alpha_k^{(1)} \alpha_l^{(1)} R_{ijkl},$$

where

$$R_{ijkl} = \langle [[[Q_i(T_1 + T_2 + T_3), Q_j(T_1 + T_2)], Q_k(T_1)], Q_l(0)] \rangle.$$

This can be reduced to the following expression within the approximation where only the first order (in terms of anharmonic coefficients $g^{(i)}$'s) contribution is included;

$$R_{ijkl} = -\frac{i}{\hbar} \frac{g^{(4)}_{ijkl} S_{ijkl}}{2 \cdot 4!} r_{ijkl},$$

where

$$r_{ijkl} = \int_{T_1+T_2}^{T_1+T_2+T_3} \mathrm{d}t \sum_{i,j,k,l} D_i(T_1 + T_2 + T_3, t) \times D_j(t, 0) D_k(t, T_1) D_l(t, T_1 + T_2).$$

This is the essential result of this paper, and can be regarded as a generalization of Eq. (3.4) of Ref. [6]. The fifth-order version of this result was first presented in Refs. [11,6] and then reproduced through other ways of calculations [33,61].

In the above, S_{ijkl} is the vertex symmetry factor, which is defined by

$$S_{ijkl} = \begin{cases} 1 & (i,j,k,l) = \text{a permutation of } (a,b,c,d), \\ 2! & (i,j,k,l) = \text{a permutation of } (a,a,b,c), \\ 3! & (i,j,k,l) = \text{a permutation of } (a,a,a,b), \\ 4! & (i,j,k,l) = (a,a,a,a), \\ 2!2! & (i,j,k,l) = \text{a perumtation of } (a,a,b,b), \end{cases}$$

where a, b, c, d designate all different modes. For example, we have

$$\sum_{i,j,k,l} \frac{g^{(4)}_{ijkl} S_{ijkl}}{2 \cdot 4!} = \frac{1}{2} g,$$

for both the anharmonic potentials

$$V_{\mathrm{AH}}(Q) = \frac{g}{4!} Q_1^4,$$

and

$$V_{\mathrm{AH}}(Q) = \frac{g}{2!2!} Q_1^2 Q_2^2.$$

The propagator is defined by

$$D_j(t,s) = \theta(t-s) \frac{\hbar}{i M_j \zeta_j} \mathrm{e}^{-\Gamma_j (t-s)/2} \sin[\zeta_j (t-s)], \quad (3)$$

where $\theta(t)$ is the Heavyside step function and

$$\zeta_j = \sqrt{\Omega_j^2 - \Gamma_i^2/4}.$$

Note that ζ_j can be imaginary for $\Omega_j < \Gamma_j/2$. In the above M_j is an effective mass.

The frequency-domain signal to be discussed below is the absolute value of the 2D Fourier transform of the impulse response at $T_2 = 0$ (i.e., $I(\omega_1, \omega_3) = |\bar{I}(\omega_1, \omega_3)|$),

$$\bar{I}(\omega_1, \omega_3) = \int_0^\infty \mathrm{d}T_1 \int_0^\infty \mathrm{d}T_3 \, \mathrm{e}^{\mathrm{i}\omega_1 T_1 + \mathrm{i}\omega_3 T_3} \times R(T_1, T_2 = 0, T_3).$$

Here, we have set $T_2 = 0$; this time configuration is the Raman echo type, but does not distinguish rephasing (echo) and nonrephasing (virtual echo) Raman coherence paths.

By noting the reduction formula,

$$\sin x_1 \sin x_2 \sin x_3 \sin x_4 = \frac{1}{8} \sum_{\varepsilon_2, \varepsilon_3, \varepsilon_4 = \pm 1} (-1)^{\varepsilon_2 + \varepsilon_3 + \varepsilon_4} \times \cos(x_1 + \varepsilon_2 x_2 + \varepsilon_3 x_3 + \varepsilon_4 x_4),$$

we can obtain an analytical expression for $\bar{I}(\omega_1, \omega_3)$ as given in Appendix A.

3. Spontaneous manifestation of the Darling–Dennison coupling

The bilinearly coupled identical oscillators (local modes) can be diagonalized, i.e.,

$$\begin{aligned} V_{\mathrm{h}} &= \tfrac{1}{2}\omega^2(x_1^2 + x_2^2) + \Delta x_1 x_2 \\ &= \tfrac{1}{2}(\omega^2 - \Delta)Q_1^2 + \tfrac{1}{2}(\omega^2 + \Delta)Q_2^2 \\ &\equiv \tfrac{1}{2}\Omega_1^2 Q_1^2 + \tfrac{1}{2}\Omega_2^2 Q_2^2, \end{aligned}$$

where, with $d = \Delta/(2\omega)$,

$$\Omega_1 \simeq \omega - d,$$

$$\Omega_2 \simeq \omega + d.$$

In the above the normal modes have been introduced as

$$Q_1 = \tfrac{1}{\sqrt{2}}(x_1 - x_2), \qquad Q_2 = \tfrac{1}{\sqrt{2}}(x_1 + x_2).$$

When the local modes have quartic self-interactions, the D–D coupling appears for the normal modes, i.e.,

$$V_{\mathrm{ah}} = \frac{g}{4!}(x_1^4 + x_2^4) \tag{4}$$

$$= V_{\mathrm{SQ}} + V_{\mathrm{DD}}, \tag{5}$$

where the self–quartic and D–D couplings are given by

$$V_{\mathrm{SQ}} = \frac{g}{2 \cdot 4!}(Q_1^4 + Q_2^4).$$

$$V_{\mathrm{DD}} = \frac{g}{2 \cdot 4!} 6 Q_1^2 Q_2^2.$$

Harmonic potential coupling between modes is not necessary since identical bonds are usually coupled through the kinetic energy operator in center of mass coordinates [51]. Any nonzero coupling (whether potential or kinetic) is sufficient to completely mix identical bond oscillators into symmetric and anti-symmetric normal modes. It is usually found that kinetic coupling dominates, but the potential coupling is not negligible [47]. The quadratic coupling strength alters the normal coordinates for similar bond oscillators attached to different functional groups, but does not generate 2D cross-peaks in the absence of higher order coupling in any case. Since the origin of the coupling is irrelevant for calculation of the 2D spectrum in the model used here, potential coupling is assumed. The origin of the coupling does matter for a priori prediction of the coupling strength.

4. Single-mode case

In this section, we present numerical results for a single-mode case to provide the basis for understanding the mode coupled case presented in the next section.

We specifically consider a mode at frequency $\Omega_1 = 600$ cm^{-1} with the damping constant (or FWHM) $\Gamma_1 = 20$ cm^{-1}. In this case,

$$\bar{I}(\omega_1, \omega_3) \propto F(1\,1\,1\,1),$$

where the function $F(1\,1\,1\,1)$ is the abbreviation of $F(\zeta_1, \Gamma_1; \zeta_1, \Gamma_1; \zeta_1, \Gamma_1; \zeta_1, \Gamma_1)$ given in Appendix A. The logarithm of the absolute value of the right-hand side is shown in Fig. 2.

The complex 2D spectrum has a symmetry $\bar{I}(\omega_1, \omega_3) = \bar{I}(-\omega_1, -\omega_3)^*$ required by the real time domain impulse response from which it is derived. The absolute value display has a twofold rotational symmetry about the origin. There are four

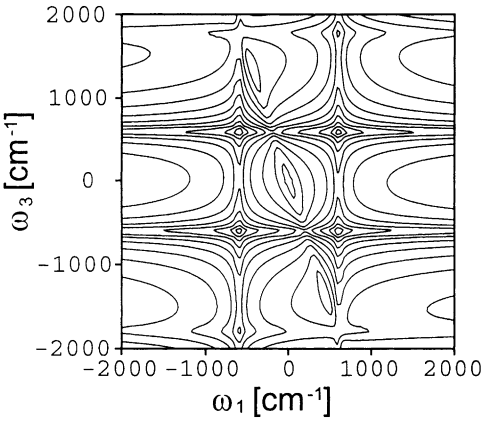

Fig. 2. 2D signal for a single mode system with a mode characterized by the parameters ($\Omega_1 = 600$, $\Gamma_1 = 20$) in the unit cm^{-1}. The logarithm of the absolute value of the Fourier-transformed quantity $\bar{I}(\omega_1, \omega_3)$ is plotted.

types of peaks in Fig. 2. These are illuminated by the analytical result. The function $F(1111)$ can be expressed as,

$$F(1111) = 2\frac{\zeta_1^4[6\Gamma_1 - i(3\omega_1 + \omega_3)]}{\prod_{s=\pm1}\{[\Gamma_1 - i(\omega_1 - s\zeta_1)][\Gamma_1 - i(\omega_3 - s\zeta_1)][3\Gamma_1 - i(\omega_3 - s3\zeta_1)]\}}.$$

The two symmetry-related peaks at $\pm(\Omega_1, \Omega_1)$ are nonrephasing (the frequencies have the same sign) with imaginary amplitude $\pm i\Omega_1/(8\Gamma_1^2)$ in the zero damping limit; the two rephasing peaks at $\pm(\Omega_1, -\Omega_1)$ have equal and opposite frequencies but twofold smaller imaginary amplitude $\pm i\Omega_1/(16\Gamma_1^2)$ in the same limit; the peaks at $\pm(\Omega_1, 3\Omega_1)$ have sixfold weaker imaginary amplitude $\pm i\Omega_1/(48\Gamma_1^2)$ in the limit because the 3 quanta damping is three times larger than for the rephasing peaks; and those at $\pm(\Omega_1, -3\Omega_1)$ with a far weaker real amplitude $-1/(48\Gamma_1)$ in the limit. These real amplitude peaks are closely connected to damping as can be seen by the vanishing resonant $F(1111)$ numerator in the zero damping limit. Off-diagonal peaks with opposite real/imaginary character to the diagonal peaks also occur in 2D NMR [36].

Off resonance, the 2D spectrum has dispersion line shapes. For example, the line $\omega_3 = \Omega_1$ exhibits a real dispersion line shape $(3\omega_3 + \Omega_1)/(16\Gamma_1\Omega_1^3(\omega_1^2 - \Omega_1^2))$ far off the resonance at $\omega_1 = \Omega_1$. The physical significance of these dispersion line shapes is not yet clear. Frequency-resolved third-order Raman line shapes have long been known to have a dispersion component around the Raman resonance [62] which is required by nonlinear causality [63]. However, the procedure for the scan and Fourier transform have a strong in influence on the 2D line shape [36,42,64] and it is possible to introduce artificial dispersion line shapes by Fourier transformation [65]. This can become a nasty problem in 2D spectroscopy because a broad dispersion line shape resulting from the first Fourier transformation can be placed on top of the absorption mode spectrum by the second Fourier transform. A better display might significantly improve 2D Raman resolution.

The position of the peaks can be understood from double-sided Feynman diagrams (see Fig. 3). The black dot stands for an interaction with the laser field through $\alpha_1^{(1)}$, implying one-quantum transition for the mode. The cross stands for the anharmonic transition (Q_1^4), which implies zero-, two-, or four-quantum transition for the mode. The diagrams in which some of the black dots and the cross are moved down also contribute the signal. As explained in Ref. [6], the cross can be placed only during T_3; there are 32 diagrams to be considered and two examples are shown in Fig. 3. In the present case T_2 is assumed to be zero.

If we look at the upper diagram, the factor $e^{-i\Omega_1 T_1}$ is associated with the period T_1. This suggests the pole at $\omega_1 = \pm\Omega_1$. Considering all the other possible diagrams, we see that the pole should be at $\omega_1 = \pm\Omega_1$.

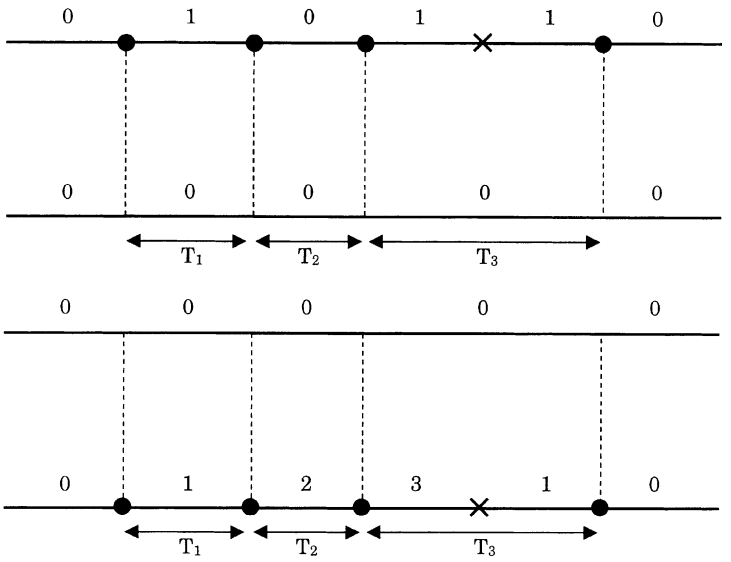

Fig. 3. Double-sided Feynman diagrams for the single-mode system with the fourth-order anharmonic interaction. We set $T_2 = 0$ in this paper. The upper line represents time evolution of the left-hand side wave function (ket) whereas the lower represents the right-hand side (bra). We assume the system is initially in the ground state denoted by zero. The black dot stands for the laser interaction which changes the oscillator state from i to $i+1$ or vice versa.

In the lower diagram, the factor $\int_0^{T_3} \mathrm{d}t\, \mathrm{e}^{-\mathrm{i}3\Omega_1 t} \times \mathrm{e}^{-\mathrm{i}\Omega_1(T_3-t)}$ is associated for the period T_3. This suggests the poles at $\omega_3 = \pm\Omega_1$ and $\pm 3\Omega_1$. After considering all the other possible diagrams, we see that the pole should be at $\omega_3 = \pm\Omega_1, \pm 3\Omega_1$

5. Two-mode case

In this section, we present numerical results for a two-mode system and demonstrate how the symmetry of the peak positions can reveal the coupling mechanism, e.g., the cross-peak is the signature for the D–D coupling while not for the S–Q coupling.

The system dealt with in this section is characterized by two identical local modes with self–quartic interactions. Due to the harmonic coupling, the two identical degrees of freedom (local mode picture) can also be treated in terms of two normal coordinates at two different frequencies instead (normal mode picture), which are, in this example, $\Omega_1 = 400$ and $\Omega_2 = 600$ cm^{-1}. The FWHM is 20 for the two modes.

To emphasize the relation between the peak symmetry and the coupling mechanism, we depicted the signals in Fig. 4 for the following three cases: (a) $V_{\mathrm{AH}} = V_{\mathrm{SQ}}$, (b) $V_{\mathrm{AH}} = V_{\mathrm{DD}}$, and (c) $V_{\mathrm{AH}} = V_{\mathrm{ah}} (= V_{\mathrm{SQ}} + V_{\mathrm{DD}})$.

The top plot (a) for the system with only the S–Q coupling shows the absolute value of the quantity,

$$\bar{I}(\omega_1,\omega_3) \propto g\left[\left(\frac{\alpha_1^{(1)}}{M_1\zeta_1}\right)^4 F(1111) + \left(\frac{\alpha_2^{(1)}}{M_2\zeta_2}\right)^4 F(2222)\right].$$

The factor $\alpha_i^{(1)}/(M_i\zeta_i)^2$ corresponds to the oscillator strength in the third-order signal, where M_i is the effective mass for the mode introduced in Eq. (3). Here and hereafter, we set this to be independent of mode species, i.e. $(\alpha_i^{(1)}/(M_i\zeta_i))^2 = 1$ for simplicity. This expression has poles at

$$\omega_1 = \pm\Omega_1, \quad \text{or} \quad \pm\Omega_2,$$

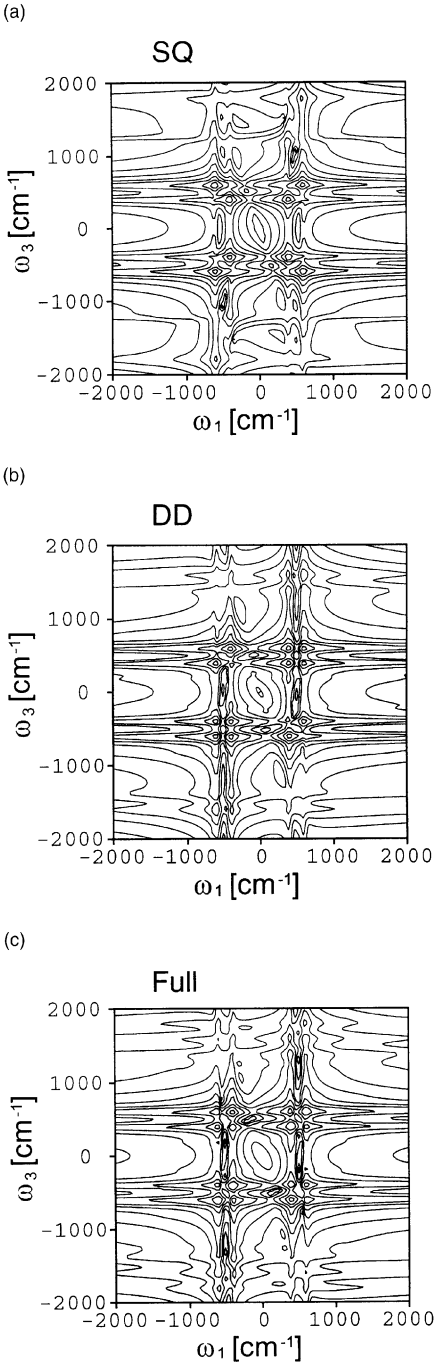

Fig. 4. 2D signal for a model system with two modes characterized by the parameters ($\Omega_1 = 400$, $\Omega_2 = 600$, $\Gamma_1 = \Gamma_2 = 20$) in the unit cm^{-1} (log plots): (a) the contribution from the self–quartic interactions, (b) the contribution from the D–D interaction, (c) the full signal.

$$\omega_3 = \pm\Omega_1, \pm\Omega_2, \pm 3\Omega_1, \quad \text{or} \quad \pm 3\Omega_2.$$

As expected from these positions of poles and from the discussion in the previous section, the plot shows diagonal and second-overtone peaks where the overtone peaks in the second and the fourth quadrants are small; there should be no cross-peaks. The physical interpretation is in parallel with that in the previous section (see also the discussion for (b) below).

The midplot (b) is for the system with only the D–D coupling, where we see some cross-peaks. By examining the analytical expression in the frequency domain given in Appendix A, we found that $\bar{I}(\omega_1, \omega_3)$ has poles at

$$\omega_1 = \pm\Omega_1, \quad \text{or} \quad \pm\Omega_2,$$

$$\omega_3 = \pm\Omega_1, \pm\Omega_2, \pm(2\Omega_1 \pm \Omega_2), \quad \text{or} \quad \pm(\Omega_1 \pm 2\Omega_2),$$

and thus there should be cross-peaks. The relative intensities among peaks can also be understood by examining the damping constant and the residue associated with each pole as we did in the previous section. We emphasize here that the diagonal peaks in the second and the fourth quadrants are extremely small.

The physical origin for these peaks can be understood by considering analytical factors associated with double-sided Feynman diagrams. As examples, two diagrams are shown in Fig. 5. In these diagrams quantum states for the modes 1 and 2 are denoted (n_1, n_2) and we assume that the system is initially in the ground state (0,0). The black dot stands for an interaction with the laser field through $\alpha_1^{(1)}$ or $\alpha_2^{(1)}$, implying one-quantum transition for either 1 or 2 mode. The cross stands for the anharmonic transition $(Q_1^2 Q_2^2)$, which implies zero- or two-quantum transition for both modes. The diagrams in which some of the black dots and the cross are moved down also contribute the signal. As explained in Ref. [6], the cross can be placed only during T_3; there are 32 diagrams to be considered without discriminating quantum states denoted by (n_i, n_j).

The factor $e^{-i\Omega_1 T_1}$ is associated with the state (1,0) appearing in the period T_1 of Fig. 5(a) and this factor leads to the pole at $\omega_1 = \pm\Omega_1$. As in

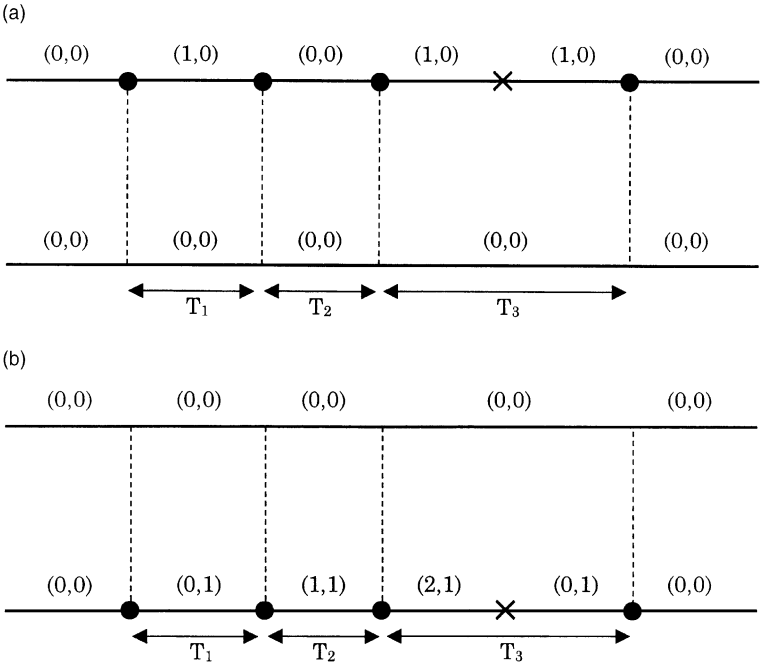

Fig. 5. Double-sided Feynman diagrams for the system with the anharmonic interaction $V_{AH} = V_{DD}$, where $T_2 = 0$.

Fig. 5(b), there are also contributions from the state (0,1) in the T_1 period, which lead to the poles at $\omega_1 = \pm\Omega_2$. In this way, we see that the pole should be at $\omega_1 = \pm\Omega_1$, or $\pm\Omega_2$.

In similar manner, considering the factor associated with the T_3 period in Fig. 5(a), we find that there should be the poles at $\omega_3 = \pm\Omega_1$. With the T_3 period of Fig. 5(b), the factor $\int_0^{T_3} dt\, e^{i(2\Omega_1+\Omega_2)t} \times e^{i\Omega_2(T_3-t)}$ is associated; this factor leads to the poles at $\omega_3 = \pm\Omega_2$ and $\pm(2\Omega_1 + \Omega_2)$. After considering all the other possible diagrams, we see that the pole should be at $\omega_3 = \pm\Omega_1, \pm\Omega_2, \pm(2\Omega_1 \pm \Omega_2)$, or $\pm(\Omega_1 \pm 2\Omega_2)$.

In summary, (i) the off-diagonal cross-peaks arise directly from the D–D coupling, (ii) the diagonal peaks in the second and the fourth quadrants arise directly from the S–Q coupling and (iii) the diagonal peaks in the first and the third quadrants come from both couplings. As the result, we can assign each peak for the full potential system in Fig. 4(c) where $\bar{I}(\omega_1, \omega_3)$ is given by the sum of those in (a) and (b); the weak diagonal peaks in the first and third quadrants is the result of negative interference of the D–D and S–Q couplings.

6. Signal from methylene chloride

We present below signals calculated by using some experimental parameters for methylene chloride [47,50]. The CH stretch vibrations in methylene halides are infrared and Raman active. These two local modes in methylene chloride can be parameterized as

$$\begin{aligned} &\omega = 3143.3, \\ &d = 31, \\ &\frac{g}{8}\left(\frac{\hbar}{2M\omega}\right)^2 = -31.6(\equiv x_{ss}), \end{aligned} \tag{6}$$

in the unit cm^{-1}. Here, M is the effective mass of the two identical local modes, i.e., $M_1 = M_2 = M$. Room temperature liquid line widths are about 36 cm^{-1} (FWHM) for the (0,0) to (1,1) infrared transition in all methylene halides, i.e., we employ

$\Gamma_1 = \Gamma_2 = 36.$

(In the following numerical results, we set that the oscillator strength $(\alpha_i^{(1)}/(M_i\zeta_i))^2 = 1$ for simplicity, although, in principle, it is possible to obtain this ratio from the high resolution experimental data.)

Fig. 6 shows the overall signal for the methylene chloride case. The previous numerical plots are all log plots while plots in Figs. 6–8 are nonlog plots, i.e., the absolute value of $\bar{I}(\omega_1, \omega_3)$ is directly shown; we concentrate on strong peaks and ignore relatively small first and third overtone peaks. Since the mode frequencies are larger compared to FWHM Γ_i and the separation d, we cannot obtain details from this plot except for the positions of four broad peaks. In this case, magnification of each broad peaks reveals new features; the broad peaks in the first and the second quadrants are magnified in Figs. 7 and 8, respectively.

The magnified plots in Figs. 7 and 8 show similar features to those observed in Fig. 4, as expected, i.e., the diagonal peaks in the second and the fourth quadrants and the cross-peaks are directly from the S–Q coupling and from the D–D coupling, respectively, while the diagonal peaks in the first and the third quadrants come from both the couplings. These results show that interpreta-

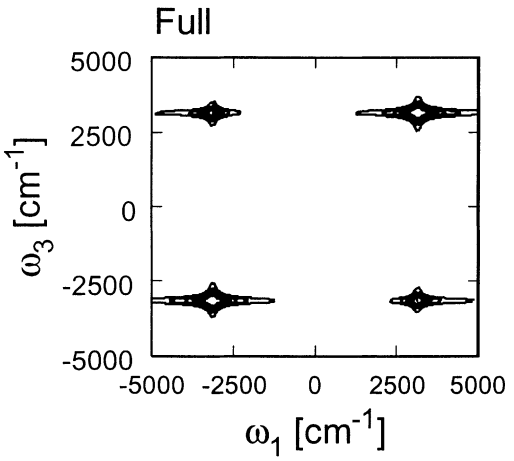

Fig. 6. 2D overall signal from anharmonic coupling of the two CH stretch vibrations at the frequency $\Omega = 3143$ in the unit cm^{-1} (nonlog plot). The two normal mode frequencies are split, i.e., $\Omega_1 = 3112$, $\Omega_2 = 3174$. The corresponding FWHM in liquid state is given by $\Gamma_1 = \Gamma_2 = 36$.

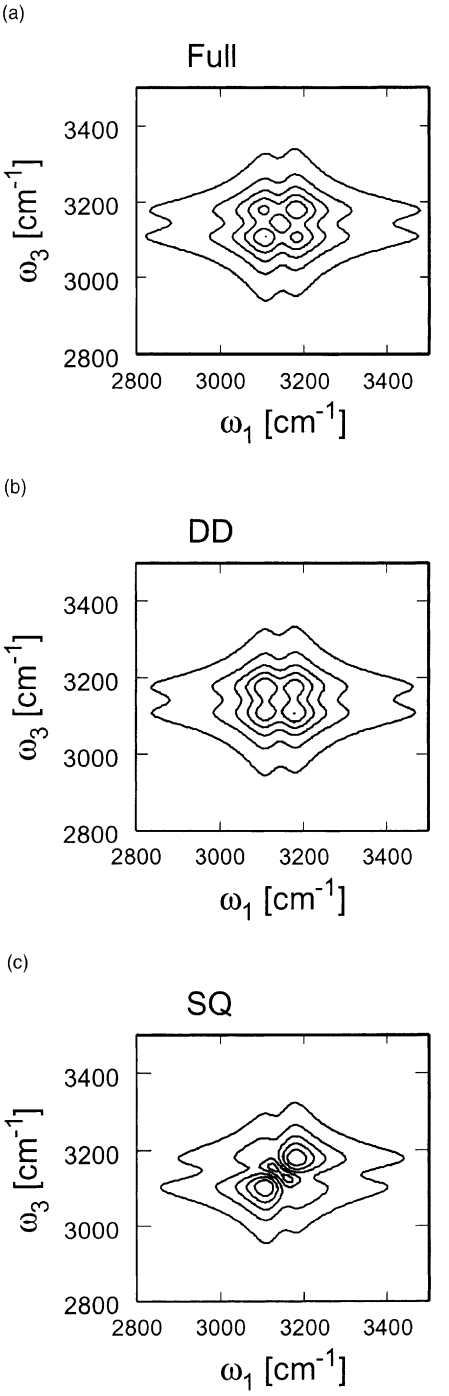

Fig. 7. 2D signal from anharmonic coupling of the two CH stretch vibrations (in the first quadrant): (a) the full signal, (b) the contribution from the D–D interaction, (c) the contribution from the self–quartic interactions.

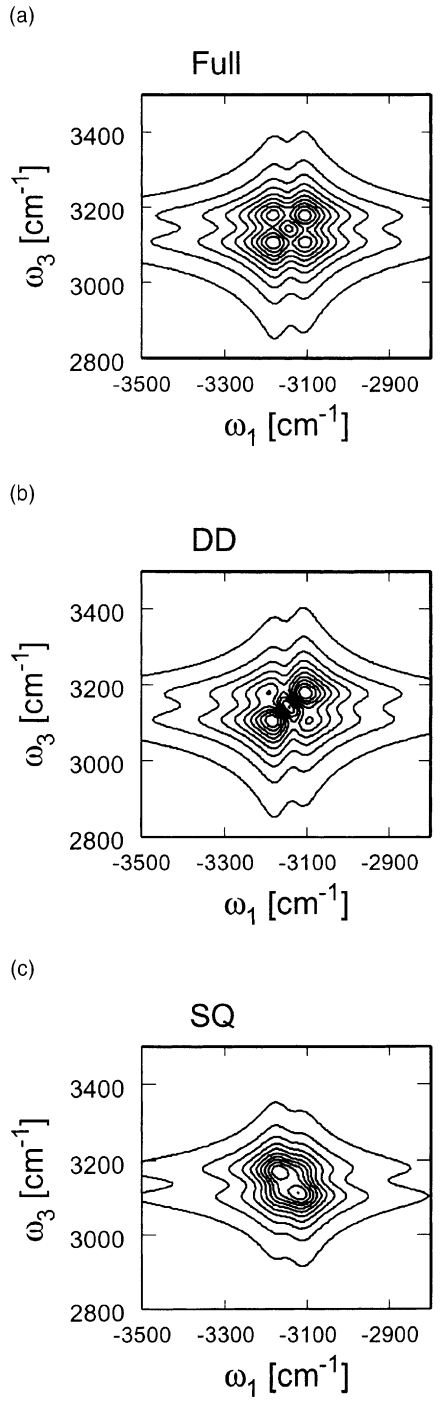

Fig. 8. 2D signal from anharmonic coupling of the two CH stretch vibrations (in the second quadrant): (a) the full signal, (b) the contribution from the D–D interaction, (c) the contribution from the self–quartic interactions.

tions given in the previous section can be invoked also in this real typical example.

7. Discussion

Even by the one-dimensional (1D) spectroscopy, we can sometimes observe anharmonicity of liquids as peak splittings [50,66], which indicate the existence of anharmonicity or nonlinearity. To determine the coupling mechanism or the form of the coupling Hamiltonian, however, more information is often required. In 2D spectroscopy, we clearly have more information. For example, we can consider symmetry of peak patterns. Owing to this, we can clearly differentiate the D–D and S–Q coupling in our demonstration by noting the cross- and diagonal-peaks.

In 1D spectroscopy, these coupling mechanism can be extracted from the fundamental and overtone spectra [45,50]. The 2D spectrum provides access to the levels observed in the overtone spectrum at frequencies near the fundamental by successive single quantum transitions, which may confer an advantage in cases where the overtone is forbidden by symmetry, intrinsically weak, or obscured by other transitions. This feature of 2D spectroscopy may allow more extensive testing of local mode models for a variety of low frequency vibrations in large molecules, but a separation into absorption and dispersion mode spectra will be needed to gain any advantage over conventional double resonance methods.

It is possible that predictions of the kinetic energy coupling between bonds from structural information might ultimately be inverted to extract structural information from mechanical couplings in 2D spectra if the anharmonic bond potentials can be assumed known with sufficient accuracy. The simple model presented here considers only the lowest order effect of anharmonicity, but demonstrates that the systematic pattern of couplings is reflected in a systematic pattern of peaks in the 2D spectrum. More detailed investigation of local mode models (which include anharmonic frequency shifts of the peaks, anharmonic intensity borrowing through nonresonant interactions, Morse oscillator relationships between cubic and

quartic local mode anharmonicity, and kinetic coupling for a variety of geometries) are desirable to determine whether such a strategy may become feasible. The extent to which such mechanical couplings may interfere with the dipole–dipole couplings (already explored at short range for nearly identical oscillators) merits investigation.

The contributions from the different orders of anharmonicity can be disentangled in higher order spectroscopy, since higher order spectroscopy possesses the selectivity in the order of anharmonicity; the third-order anharmonicity can be investigated by fifth-order spectroscopy while fourth-order anharmonicity can be investigated by seventh-order spectroscopy [6]. For example, in the seventh-order spectroscopy, the Fermi resonance (the third-order anharmonicity) plays no role in the lowest order theory of the seventh-order signal and we can concentrate only on the D–D interaction, while both contributions are sometimes allowed in lower order spectroscopy.

The above consideration implies the need for the further development of the theory of nonlinear multi-dimensional spectroscopy based on the Brownian oscillator model especially for the molecular-level understanding of intramolecular modes.

Acknowledgements

This work is supported by a Grant-in-Aid on priority Area of "Chemical Reaction Dynamics in Condensed Phases" (10206210) and the Grant-in-Aid for Scientific Research (B) (12440171) both from the Japanese Ministry of Education, Science, Sports and Culture. D.M.J. thanks the NSF, Packard, and Sloan Foundations for support.

Appendix A

For the system with $V_{AH} = V_{DD}$, the signal is given through

$$\bar{I}(\omega_1,\omega_3) = f(1122) + f(1212) + f(1221) + f(2112) + f(2121) + f(2211),$$

while

$$\bar{I}(\omega_1,\omega_3) = f(1111) + f(2222),$$

for the system with $V_{AH} = V_{SQ}$. For the system with $V_{AH} = V_{ah}$, $\bar{I}(\omega_1,\omega_3)$ is given by the sum of the above two expressions.

Here, the function f is defined by

$$f(ijkl) = \left(\frac{\hbar}{i}\right)^4 \frac{F(\zeta_i,\Gamma_i;\zeta_j,\Gamma_j;\zeta_k,\Gamma_k;\zeta_l,\Gamma_l)}{M_iM_jM_kM_l\zeta_i\zeta_j\zeta_k\zeta_l},$$

where

$$F(\zeta_i,\Gamma_i;\zeta_j,\Gamma_j;\zeta_k,\Gamma_k;\zeta_l,\Gamma_l) = \frac{1}{8}\sum_s G_s(\zeta_i,\Gamma_i;\zeta_j,\Gamma_j;\zeta_k,\Gamma_k;\zeta_l,\gamma_l).$$

The summation is taken over the following set;

$$(s_1,s_2,s_3,s_4) = \begin{cases} (-1,1,1,1), \\ (1,-1,1,1), \\ (1,1,-1,1), \\ (1,1,1,-1), \\ (1,-1,-1,-1), \\ (-1,1,-1,-1), \\ (-1,-1,1,-1), \\ (-1,-1,-1,1). \end{cases}$$

Here, the function G_s is defined as

$$G_s(\zeta_1,\Gamma_1;\zeta_2,\Gamma_2;\zeta_3,\Gamma_3;\zeta_4,\Gamma_4) = s_1\frac{(\Gamma_{234}-i\omega_3)[(\Gamma_2-i\omega_1)(\Gamma_1-i\omega_3)+s_2\zeta_1\zeta_2]+\zeta_{234}[(\Gamma_2-i\omega_1)\zeta_1-(\Gamma_1-i\omega_3)s_2\zeta_2]}{\Pi_{s=\pm1}[\{\Gamma_1-i(\omega_3-s\zeta_1)\}\{\Gamma_2-i(\omega_1-s\zeta_2)\}\{\Gamma_{234}-i(\omega_3-s\zeta_{234})\}]},$$

where

$$\Gamma_{234} = \Gamma_2+\Gamma_3+\Gamma_4,$$

$$\zeta_{234} = s_2\zeta_2+s_3\zeta_3+s_4\zeta_4.$$

References

[1] Y. Tanimura, S. Mukamel, J. Chem. Phys. 99 (1993) 9496.
[2] K. Tominaga, K. Yoshihara, Phys. Rev. Lett. 74 (1995) 3061.
[3] T. Steffen, K. Duppen, Phys. Rev. Lett. 76 (1996) 1224.
[4] A. Tokmakoff, G.R. Fleming, J. Chem. Phys. 106 (1997) 2569.
[5] K. Okumura, Y. Tanimura, J. Chem. Phys. 107 (1997) 2267.
[6] K. Okumura, Y. Tanimura, J. Chem. Phys. 106 (1997) 1687.
[7] S. Hahn, K. Park, M. Cho, J. Chem. Phys. 111 (1999) 4121.
[8] Y. Tanimura, Chem. Phys. 233 (1998) 217.
[9] K. Park, M. Cho, J. Chem. Phys. 112 (2000) 10496.
[10] A. Tokmakoff, M.J. Lang, D.S. Larsen, G.R. Fleming, V. Chernyak, S. Mukamel, Phys. Rev. Lett. 79 (1997) 2702.
[11] K. Okumura, Y. Tanimura, Chem. Phys. Lett. 278 (1997) 175.
[12] D.J. Ulness, J.C. Kirkwood, A.C. Albrecht, J. Chem. Phys. 108 (1998) 3897.
[13] D.A. Blank, L.J. Kaufman, G.R. Fleming, J. Chem. Phys. 111 (1999) 3105.
[14] M. Cho, D.A. Blank, J. Sung, K. Park, S. Hahn, G.R. Fleming, J. Chem. Phys. 112 (2000) 2082.
[15] D. Blank, L.J. Kaufman, G.R. Fleming, J. Chem. Phys. 113 (2000) 771.
[16] V. Astinov, K. Kubarych, C. Milne, R.J.D. Miller, Opt. Lett. 25 (2000) 853.
[17] V. Astinov, K. Kubarych, C. Milne, R.J.D. Miller, Chem. Phys. Lett. 327 (2000) 334.
[18] O. Golonzka, N. Demirdoven, A. Tokmakoff, J. Chem. Phys. 113 (2000) 9893.
[19] S. Saito, I. Ohmine, J. Chem. Phys. 108 (1998) 240.
[20] I. Ohmine, S. Saito, Acc. Chem. Res. 32 (1999) 741.
[21] T. Keyes, J.T. Fourkas, J. Chem. Phys. 112 (2000) 287.
[22] A. Ma, R.M. Stratt, Phys. Rev. Lett. 85 (2000) 1004.
[23] L. Lepetit, M. Joffre, Opt. Lett. 21 (1996) 564.
[24] J. Hybl, A.W. Albrecht, S.M.G. Faeder, D.M. Jonas, Chem. Phys. Lett. 297 (1998) 307.
[25] S.M.G. Faeder, D.M. Jonas, J. Phys. Chem. A 103 (1999) 10489.
[26] Y. Tanimura, K. Okumura, J. Chem. Phys. 106 (1997) 2078.
[27] K. Okumura, A. Tokmakoff, Y. Tanimura, Chem. Phys. Lett. 314 (1999) 488.
[28] W. Zhao, J.C. Wright, Phys. Rev. Lett. 83 (1999) 1950.
[29] W. Zhao, J.C. Wright, Phys. Rev. Lett. 84 (2000) 1411.
[30] W. Zhao, J.C. Wright, J. Am. Chem. Soc. 121 (1999) 10994.
[31] M. Cho, K. Okumura, Y. Tanimura, J. Chem. Phys. 108 (1998) 1326.
[32] K. Okumura, Y. Tanimura, Chem. Phys. Lett. 295 (1998) 298.
[33] M. Cho, in: Y. Fujimura, S.H. Lin (Eds.), Advances in Multi-photon Processes and Spectroscopy, vol. 12, World Scientific, Singapore, 1999, pp. 1–71.
[34] K. Okumura, A. Tokmakoff, Y. Tanimura, J. Chem. Phys. 111 (1999) 492.
[35] P. Hamm, M. Lim, W.F. DeGrado, R.M. Hochstrasser, Proc. Natl. Acad. Sci. USA 96 (1999) 2036.
[36] R.R. Ernst, G. Bodenhausen, A. Wokaun, Principles of Nuclear Magnetic Resonance in One and Two Dimensions, Oxford University Press, Oxford, 1987.
[37] S. Hahn, K. Kwak, M. Cho, J. Chem. Phys. 112 (2000) 4553.
[38] T. Steffen, Y. Tanimura, J. Phys. Soc. Jpn. 69 (2000) 3115.
[39] Y. Tanimura, T. Steffen, Two-dimensional spectroscopy for harmonic vibrational modes with nonlinear 20 system-bath interaction: II. Gaussian-Markovian case, J. Phys. Soc. Jpn. 69 (2000) 4095.
[40] S. Mukamel, A. Piryatinski, V. Chernyak, J. Chem. Phys. 110 (1999) 1711.
[41] S. Mukamel, A. Piryatinski, V. Chernyak, Acc. Chem. Res. 32 (1999) 145.
[42] S.M. Gallagher Faeder, D.M. Jonas, J. Phys. Chem. A 103 (1999) 10489.
[43] A. Tokmakoff, J. Phys. Chem. A 104 (2000) 4247.
[44] D.M. Dennison, Rev. Mod. Phys. 12 (1940) 175.
[45] I.M. Mills, A.G. Robiette, Mol. Phys. 56 (1985) 743.
[46] K.K. Lehmann, S.L. Coy, J. Chem. Soc. Faraday Trans. 84 (1988) 1389.
[47] G.H. Herzberg, Infrared and Raman Spectra of Polyatomic Molecules, vol. II, Krieger, Malabar, FL, 1991.
[48] D.M. Jonas, S.A.B. Solina, B. Rajaram, R.J. Silbey, R.W. Field, K. Yamanouchi, S. Tsuchiya, J. Chem. Phys. 99 (1993) 7350.
[49] M.P. Jacobson, R.W. Field, J. Phys. Chem. A 104 (2000) 3073.
[50] O.S. Mortensen, B.R. Henry, M.A. Mohammadi, J. Chem. Phys. 75 (1981) 4800.
[51] L.D. Landau, E.M. Lifschitz, Mechanics, Pergamon Press, New York, 1976.
[52] E.L. Sibert III, J.T. Hynes, W.P. Reinhardt, J. Phys. Chem. 87 (1983) 2032.
[53] D. Papousek, M.R. Aliev, Molecular Vibrational-Rotational Spectra, Elsevier Scientific, New York, 1982.
[54] J. Pliva, Collection Czechoslovak Chem. Commun. 23 (1958) 777.
[55] F. Iachello, Chem. Phys. Lett. 78 (1981) 581.
[56] F. Iachello, R.D. Levine, J. Chem. Phys. 77 (1982) 3046.
[57] O.S. van Roosmalen, F. Iachello, R.D. Levine, A.E.L. Dieperink, J. Chem. Phys. 79 (1983) 2515.
[58] S. Mukamel, Principles of Nonlinear Optical Spectroscopy, Oxford University Press, Oxford, 1995.
[59] R.L. Murry, J.T. Fourkas, T. Keyes, J. Chem. Phys. 109 (1998) 2814.
[60] R.L. Murry, J.T. Fourkas, T. Keyes, J. Chem. Phys. 109 (1998) 7913.

[61] V. Chernyak, S. Mukamel, J. Chem. Phys. 108 (1998) 5812.
[62] M.D. Levenson, N. Bloembergen, J. Chem. Phys. 60 (1974) 1323.
[63] N. Bloembergen, Nonlinear Optics, Addison-Wesley, New York, 1992.
[64] J.D. Hybl, A.W. Albrecht, S.M. Gallagher Faeder, D.M. Jonas, Chem. Phys. Lett. 297 (1998) 307.
[65] A.W. Albrecht, J.D. Hybl, S.M. Gallagher Faeder, D.M. Jonas, J. Chem. Phys. 111 (1999) 10934.
[66] K. Okumura, Y. Tanimura, J. Chem. Phys. 105 (1996) 7294.